Exploring the magnetic interaction in the photoexcited of porphyrin-lanthanide 1:1 complexes with different capping ligands

Anas Santria,[1,2] and Naoto Ishikawa[1]

[1]Graduate School of Science, Osaka University

[2]Research Center for Chemistry, National Research and Innovation Agency

1. Introduction

In the field of electronic interactions, an intriguing phenomenon has emerged—an interaction between two angular momenta: the total angular momentum arising from the f system (**J**) and the orbital angular momentum originating from the photoexcited cyclic π electronic system (**L**). This interaction, termed **J**-**L** interaction, has been observed experimentally in the paramagnetic phthalocyaninato/ porphyrinato lanthanide complex. Our group's research is devoted to uncovering the intricacies of this interaction.

Our work has focused on investigating the **J**-**L** interaction in double- and single-decker phthalocyaninato/ porphyrinato complexes, featuring lanthanide ions with $4f^8$ and $4f^9$ configurations. [1] We have investigated the interaction through careful experimental analysis using magnetic circular dichroism (MCD). In our prior investigations, we explored the interaction in single-decker compounds encompassing various lanthanide ions ranging from terbium to ytterbium. Furthermore, our investigation has integrated computational chemistry methods to deepen our understanding. *Ab initio* calculations have revealed two manifestations of the interaction: ferromagnetic-type and antiferromagnetic-type interactions. To date, we have observed the ferromagnetic-type interaction in terbium, erbium, and ytterbium complexes, whereas the antiferromagnetic-type interaction has been observed in dysprosium complex.[2]

Building upon this groundwork, using computational chemistry, our study explores the electronic structure of lanthanide-monoporphyrin complexes with different capping ligands, such as 1,4,7,10-tetraazadodecane (L1), 4,10-diaza-12-crown-4 ether (L2), 1-aza-12-crown-4 ether (L3), and 12-crown-4 ether (L4), as illustrated in Figure 1. We argue that the choice of capping ligand influences the **J**-**L** interaction.

Through this examination, our objective is to elucidate the interplay between angular momenta and the impact of ligand restraint on electronic structure, thereby enriching our understanding of the **J**-**L** interaction.

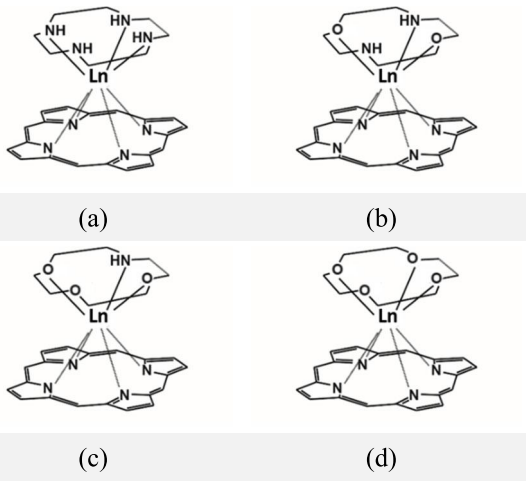

Figure 1: Structures of (a) $[Dy(Por)(L1)]^+$, (b) $[Dy(Por)(L2)]^+$, (c) $[Dy(Por)(L3)]^+$, and (d) $[Dy(Por)(L4)]^+$.

2. Computational Methods

The geometry structures of $[Dy(Por)(L)]^+$ (Por = porphyrine; L = 1,4,7,10-tetraazadodecane (L1), 4,10-diaza-12-crown-4 ether (L2), and 1-aza-12-crown-4 ether (L3), 12-crown-4 ether (L4) were constructed using the Avogadro program.[3] Subsequently, the geometry optimization process was carried out employing *Gaussian 16*, revision C.01 [4] at the B3LYP level of theory. The basis set 6-31G(d,p) was utilized for C, H, N, and O atoms [5], while Stuttgart RSC 1997 basis sets were employed for metal ion [6].

For the determination of electronic structures, spin-orbit states (SO), and oscillator strength of the optimized geometries, a series of computational methods were employed. Initially, completed active space self-consistent field (CASSCF) were performed, followed by restricted active space state interaction (RASSI) and Single_Aniso modules, using OpenMolcas version 23.10. [7] In these calculations, the basis set ANO-RCC-VQZP and ANO-RCC-VDZP was applied for Dy and the donor atoms (N and O), respectively, while ANO-RCC-MB was employed for the remaining atoms (C, H, N).

3. Results and Discussion

The calculations initially focused on the states associated with the $4f^9$ electronic configuration, eferred to as the ground states. Following this, utilizing these findings as a starting point, the computations for the π–π* excited states were carried out. This involved considering the two highest occupied molecular orbitals (HOMOs) and the two lowest unoccupied molecular orbitals (LUMOs) of the porphyrin π system, thus broadening the active space for analysis.

3.1 Ground Multiplet States

To obtain the ground multiplet states of the $[Dy(Por)(L)]^+$ complexes, we employed a CASSCF module with 9 electrons distributed in 7 orbitals, denoted as CAS(9,7). This calculation involved 21 configurational interaction (CI) roots, yielding a total of 21 electron configurations representing the nine electrons within the seven 4f orbitals. The positioning of these seven 4f orbitals was identified between two occupied π and two unoccupied π orbitals. Given the successful arrangement of these 4f and pi orbitals, this configuration was chosen as the foundational setup for subsequent analyses.

Table 1 displays the eight lowest doublet spin-orbit states corresponding to the ground multiplet states of the $[Dy(Por)(L)]^+$ complexes. The change of nitrogen with oxygen at the capping ligand significantly altered the sublevel structure of the complexes. The lowest substate in $[Dy(Por)(L1)]^+$, $[Dy(Por)(L2)]^+$, and $[Dy(Por)(L4)]^+$ predominantly comprises more than 90% $|\pm 11/2\rangle$, with negligible contributions below 10% for other J_z values. These results are consistent with our previous findings.[2,8] For $[Dy(Por)(L3)]^+$, the lowest substate primarily consists of 75% $|\pm 15/2\rangle$ and 16% $|\pm 11/2\rangle$, with insignificant contributions below 10% for other J_z values. This signifies a notable shift in the dominant J_z value from $|\pm 11/2\rangle$ in $[Dy(Por)(L1)]^+$, $[Dy(Por)(L2)]^+$, and $[Dy(Por)(L4)]^+$ to $|\pm 15/2\rangle$ in $[Dy(Por)(L3)]^+$. The second lowest substates in all complexes are predominantly $|\pm 13/2\rangle$. They are separated by around 8 cm^{-1}, 22 cm^{-1}, 38 cm^{-1}, and 45 cm^{-1}, respectively, from the lowest ground state. This illustrates that the energy separation between the lowest and second lowest substates increases as the number of nitrogen donor atoms decreases. Considering the composition of the lowest substate, $[Dy(Por)(L3)]^+$ lacks a prominent dominance of component $|\pm 13/2\rangle$ over other components in the second lowest substate. Consequently, it is not prudent to conclude that $|\pm 13/2\rangle$ represents the $|J_z\rangle$ for the second lowest substate. Furthermore, beyond the two lowest substates, the degree of mixing is noticeably more pronounced in the higher substates, particularly for complexes with L2 and L3 capping ligands, rendering the determination of J_z for the remaining substates considerably more intricate.

Table 1. Energy level of the dysprosium complexes extracted from CASSCF/RASSI/ SINGLE_ANISO calculations.

$[Dy(Por)(L1)]^+$		$[Dy(Por)(L2)]^+$	
Energy (cm^{-1})	States	Energy (cm^{-1})	States
0	$0.99\|\pm11/2\rangle$	0	$0.96\|\pm11/2\rangle$
8	$0.98\|\pm13/2\rangle$	22	$0.88\|\pm13/2\rangle$
121	$0.90\|\pm9/2\rangle$	100	$0.68\|\pm9/2\rangle$ $0.14\|\pm1/2\rangle$
217	$0.78\|\pm7/2\rangle$ $0.16\|\pm1/2\rangle$	158	$0.36\|\pm7/2\rangle$ $0.20\|\pm3/2\rangle$ $0.17\|\pm5/2\rangle$ $0.13\|\pm9/2\rangle$ $0.13\|\pm1/2\rangle$
242	$0.54\|\pm5/2\rangle$ $0.40\|\pm3/2\rangle$	200	$0.30\|\pm7/2\rangle$ $0.29\|\pm5/2\rangle$ $0.25\|\pm3/2\rangle$
343	$0.77\|\pm1/2\rangle$ $0.19\|\pm7/2\rangle$	269	$0.41\|\pm1/2\rangle$ $0.20\|\pm5/2\rangle$ $0.19\|\pm3/2\rangle$ $0.18\|\pm7/2\rangle$
355	$0.57\|\pm3/2\rangle$ $0.43\|\pm5/2\rangle$	323	$0.32\|\pm3/2\rangle$ $0.28\|\pm5/2\rangle$ $0.25\|\pm1/2\rangle$ $0.11\|\pm7/2\rangle$
502	$1.00\|\pm15/2\rangle$	517	$1.00\|\pm15/2\rangle$

$[Dy(Por)(L3)]^+$		$[Dy(Por)(L4)]^+$	
Energy (cm^{-1})	States	Energy (cm^{-1})	States
0	$0.75\|\pm15/2\rangle$ $0.16\|\pm11/2\rangle$	0	$0.93\|\pm11/2\rangle$
38	$0.57\|\pm13/2\rangle$ $0.23\|\pm9/2\rangle$ $0.10\|\pm7/2\rangle$	45	$0.95\|\pm13/2\rangle$
84	$0.24\|\pm11/2\rangle$ $0.24\|\pm5/2\rangle$ $0.16\|\pm7/2\rangle$ $0.10\|\pm3/2\rangle$	56	$0.52\|\pm9/2\rangle$ $0.35\|\pm1/2\rangle$ $0.12\|\pm7/2\rangle$
119	$0.28\|\pm1/2\rangle$ $0.26\|\pm3/2\rangle$ $0.13\|\pm11/2\rangle$ $0.11\|\pm7/2\rangle$	102	$0.47\|\pm3/2\rangle$ $0.44\|\pm5/2\rangle$
144	$0.39\|\pm1/2\rangle$ $0.18\|\pm3/2\rangle$ $0.14\|\pm5/2\rangle$ $0.11\|\pm11/2\rangle$	123	$0.45\|\pm7/2\rangle$ $0.41\|\pm9/2\rangle$ $0.14\|\pm1/2\rangle$
215	$0.24\|\pm9/2\rangle$ $0.21\|\pm3/2\rangle$ $0.14\|\pm7/2\rangle$ $0.14\|\pm11/2\rangle$ $0.11\|\pm5/2\rangle$	223	$0.50\|\pm1/2\rangle$ $0.43\|\pm7/2\rangle$
225	$0.28\|\pm5/2\rangle$ $0.21\|\pm1/2\rangle$ $0.20\|\pm7/2\rangle$ $0.16\|\pm3/2\rangle$	231	$0.51\|\pm5/2\rangle$ $0.46\|\pm3/2\rangle$
353	$0.27\|\pm9/2\rangle$ $0.25\|\pm7/2\rangle$ $0.18\|\pm11/2\rangle$ $0.14\|\pm5/2\rangle$	532	$1.00\|\pm15/2\rangle$

In addition to the change in J_z, the orientation of the main magnetic axis in $[Dy(Por)(L3)]^+$ exhibits a significant deviation from that of other complexes as shown in Figure 2. Unlike $[Dy(Por)(L1)]^+$, $[Dy(Por)(L2)]^+$, and $[Dy(Por)(L4)]^+$, where the main magnetic axis aligns with the z-axis (perpendicular to the porphyrin plane), $[Dy(Por)(L3)]^+$ demonstrates an inclination of 52 degrees towards the amine of the L3 ligand. This inclination becomes even more pronounced for the main magnetic axis in the second lowest substate, reaching approximately 69 degrees from the z-axis. This observation underscores that even a slight alteration of one atom in the ligand can induce a change in symmetry, thereby impacting the orientation of the main magnetic axis of the compound.

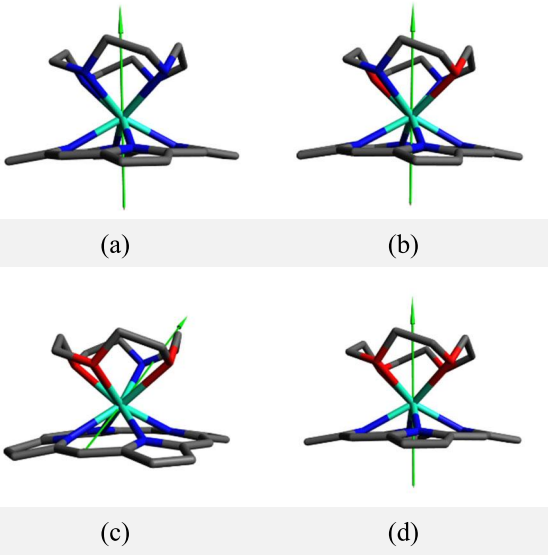

Figure 2: The main magnetic axis of the lowest J_z of $[Dy(Por)(L)]^+$ complexes ((a) $[Dy(Por)(L1)]^+$, (b) $[Dy(Por)(L2)]^+$, (c) $[Dy(Por)(L3)]^+$, and (d) $[Dy(Por)(L4)]^+$).

3.2 Excited-states

In calculating excited states, we expanded the active space utilized for the CASSCF method to include 11 orbitals, designated as CAS(13,11). The active space encompassed the seven $4f^9$ orbitals of Dy(III), along with the two highest doubly occupied π orbitals and the two lowest unoccupied π orbitals. The initial orbitals were derived from one of the 21 CI roots generated in preceding ground state calculations. To streamline the report, we will focus solely on the calculation results of $[Dy(Por)(L3)]^+$ and $[Dy(Por)(L4)]^+$, which exhibit significant differences in the main magnetic axis in the ground state.

Utilizing a total of 195 CI roots, each with a spin multiplicity of 6, in this CASSCF calculation resulted in 1170 spin-orbit states (585 doublets). Among this extensive array of SO transitions, we focused on identifying π→π* transitions associated with the Q and B bands, considering the oscillator strength of each transition. Additionally, employing the SINGLE_ANISO module, we determined the angular momenta for each SO state, as detailed in Tables 2-3.

Table 2. Selected transition energy and angular momenta of $[Dy(Por)(L4)]^+$ extracted from CASSCF/RASSI/SINGLE_ANISO calculations.

Doublet	Energy (cm^{-1})	Osc. Strength (initial doublet → final doublet)	|Lz|	|Sz|	|Jz| = |Lz + Sz|
1	0		2.91	1.48	4.39
2	17		1.27	0.62	1.89
3	47		1.83	0.96	2.79
4	66		0.32	0.17	0.49
5	79		2.41	1.25	3.66
6	204		0.06	0.01	0.07
7	218		0.07	0.02	0.09
8	340		4.98	2.50	7.48
137	31697	0.015 (8→137)	9.53	2.50	12.03
138	31708	0.015(8→138)	0.41	2.49	2.90
139	31724	0.008(3→139)	0.29	2.14	1.85
140	31733	0.008(3→140)	8.84	2.14	10.98
141	31769	0.014(1→141)	1.06	1.72	0.66
142	31781	0.014(1→142)	8.07	1.74	9.81
143	31812	0.014(2→143)	2.29	1.10	1.20
144	31817	0.014(2→144)	6.76	1.09	7.85
145	31883	0.014(4→145)	3.39	0.51	2.88
146	31884	0.014(4→146)	5.86	0.62	6.48
147	31912	0.008(5→147)	4.07	0.18	3.89
148	31912	0.008(5→148)	5.14	0.27	5.41
149	32038	0.015(7→149)	4.47	0.04	4.43
150	32038	0.015(7→150)	4.32	0.05	4.27
151	32057	0.015(6→151)	4.46	0.04	4.42
152	32058	0.015(6→152)	4.29	0.07	4.22
407	47288	2.84(1→ 407)	2.64	1.40	4.04
409	47299	2.44(1→ 409)	1.20	0.61	1.81
412	47314	1.94(2→ 412)	2.13	1.12	3.25
413	47323	2.98(2→ 413)	3.88	1.92	5.80
410	47305	2.86(3→ 410)	0.04	0.02	0.06
411	47310	1.79(3→ 411)	1.89	0.97	2.86
414	47362	2.71(4→ 414)	2.25	1.16	3.41
415	47364	2.70(4→ 415)	2.05	1.05	3.10
416	47371	2.62(5→ 416)	2.49	1.27	3.76
417	47373	2.73(5→ 417)	2.76	1.41	4.17
418	47451	3.02(6→ 418)	5.08	2.48	7.56
419	47465	3.00(6→ 419)	4.67	2.41	7.08
420	47507	2.98(7→ 420)	0.09	0.02	0.11
421	47509	2.97(7→ 421)	0.11	0.07	0.18
422	47510	2.98(8→ 422)	0.04	0.02	0.06
423	47512	2.99(8→ 423)	0.04	0.02	0.06

The selected doublet SO states of $[Dy(Por)(L4)]^+$ are listed in Table 2. Two pairs of degenerate SO states associated with the π → π* transition at the Q-band of $[Dy(Por)(L4)]^+$ were identified. The doublet states numbered 141 and 142 will be henceforth referred to as the lower and higher excited doublet SO states, respectively. The lower excited doublet SO state is distinguished by its separation of 31770 cm^{-1} from the ground SO state. Along the z-axis, the spin angular momentum (S_Z) was determined to be 1.72 $\hbar$, with an absolute value of the orbital angular momentum ($|L_Z|$) at 1.06 $\hbar$ for this doublet state. Since S_Z is proximate to that of the ground doublet SO state (1.48 $\hbar$), it is reasonable to infer that S_Z in the lower excited doublet SO state corresponds to the spin angular momentum of the dysprosium ion (S_Z(f)). However, in comparison to the ground doublet SO state, the $|L_Z|$ in this doublet has significantly decreased by 3.97 $\hbar$. This reduction is attributed to the orbital angular momentum of the π system (L_Z(π)), as previously reported.[9]

For the higher excited doublet SO state, which sits about 31781 cm^{-1} above the ground doublet SO state, the S_Z remains nearly unchanged compared to that of the ground state (1.48 $\hbar$). However, the $|L_Z|$ value in this state notably increases to around 8.07 $\hbar$. Once again, the disparity in $|L_Z|$ values indicates the presence

of $L_Z(\pi)$ in the excited state of $[Dy(Por)(L4)]^+$, aligning with previous finding. [9] Considering the decrease in the L_Z value in the lower excited doublet SO state, indicating an opposite orientation or antiparallel between $L_Z(\pi)$ and $L_Z(f)$, it can be inferred that an antiferromagnetic-type interaction exists between $L_Z(\pi)$ and $L_Z(f)$ in this compound.

Concerning the interaction magnitude (Δ_{JL}), we turn to our previous studies,[9] where this value was defined as half the energy gap between the lower and higher pairs of the excited SO doublet. In the Q band of $[Dy(Por)(L4)]^+$, the Δ_{JL} value was determined to be around 6 cm^{-1}, which overestimates the experimental result ($\Delta_{JL} = 0.39$ cm^{-1}). [10] Despite the discrepancy, it is significant to note that the opposing orientation between $L_Z(\pi)$ and $L_Z(f)$ aligns well with the experimental observations, providing further evidence for the presence of an antiferromagnetic-type **J**-**L** interaction in $[Dy(Por)(L4)]^+$.

Table 3. Selected transition energy and angular momenta of $[Dy(Por)(L3)]^+$ extracted from CASSCF/RASSI/SINGLE_ANISO calculations.

Doublet	Energy (cm^{-1})	Osc. Strength (initial doublet → final doublet)	|Lz|	|Sz|	|Jz| = |Lz + Sz|
1	0		4.52	2.28	6.80
2	34		3.59	1.80	5.39
3	78		2.93	1.46	4.39
4	118		0.60	0.30	0.90
5	137		3.34	1.70	5.04
6	250		4.66	2.34	7.00
7	272		4.61	2.31	6.92
8	296		4.81	2.41	7.22
133	31568	0.003(1→133)	4.33	2.22	6.55
142	31723	0.005(1→142)	4.57	2.24	6.81
136	31601	0.002(2→136)	3.23	1.44	4.67
143	31754	0.006(2→143)	3.67	1.83	5.50
138	31648	0.003(3→138)	3.00	1.47	4.47
144	31801	0.004(3→144)	2.96	1.49	4.45
140	31688	0.003(4→140)	0.87	0.44	1.31
147	31844	0.003(4→147)	2.70	1.37	4.07
141	31712	0.003(5→141)	3.34	1.81	5.15
148	31865	0.006(5→148)	3.77	1.82	5.59
145	31821	0.003(6→145)	4.64	2.30	6.94
150	31973	0.007(6→150)	4.74	2.40	7.14
146	31838	0.002(7→146)	3.31	1.67	4.98
151	31997	0.001(7→151)	4.69	2.35	7.04
149	31872	0.003(8→149)	4.99	2.34	7.33
152	32025	0.007(8→152)	4.51	2.42	6.93
403	46815	2.11(1→ 403)	4.48	2.26	6.74
410	47091	1.90(1→ 410)	4.30	2.17	6.47
404	46846	2.90(2→ 404)	3.70	1.86	5.56
411	47120	1.42(2→ 411)	3.45	1.73	5.18
405	46895	2.33(3→ 405)	3.01	1.49	4.50
413	47169	2.34(3→ 413)	2.96	1.47	4.43
406	46935	2.19(4→ 406)	2.22	1.10	3.32
414	47208	2.01(4→ 414)	0.94	0.47	1.41
407	46961	2.83(5→ 407)	3.50	1.79	5.29
416	47234	2.90(5→ 416)	3.63	1.86	5.49
408	47068	2.99(6→ 408)	4.74	2.38	7.12
420	47340	3.04(6→ 420)	4.78	2.40	7.18
409	47087	2.80(7→ 409)	4.54	2.28	6.82
422	47363	3.07(7→ 422)	4.72	2.37	7.09
411	47120	1.53(8→ 411)	3.45	1.73	5.18
423	47395	3.08(8→ 423)	4.85	2.44	7.29

Similar to the computations conducted for $[Dy(Por)(L4)]^+$, those for $[Dy(Por)(L3)]^+$ also yield a pair of doublet SO states associated with $\pi \rightarrow \pi^*$ transitions. These doublet SO states are separated by 31568 cm^{-1} (doublet 133) and 31723 cm^{-1} (doublet 142) from the lowest doublet SO state, as shown in Table 3. However, unlike $[Dy(Por)(L4)]^+$, where the higher-energy doublet is merely one level above the lower-energy doublet, in $[Dy(Por)(L3)]^+$, eight other doublet SO states separate the two doublets.

In doublet 133, the L_Z value undergoes a reduction of approximately 0.2, while S_Z remains relatively unchanged (2.22), yielding a J_Z value of 6.55. Conversely, in the higher doublet (doublet 142), the L_Z experiences a slight increase of 0.05, resulting in a J_Z value 0.26 larger than that in doublet 133. From this data, it can be deduced that the **J**-**L** interaction in $[Dy(Por)(L3)]^+$ has the same type with that in $[Dy(Por)(L4)]^+$, consistent with findings from experiments using MCD data. [10]

However, a significant contrast between $[Dy(Por)(L3)]^+$ and $[Dy(Por)(L4)]^+$ is in the magnitude of change in L_Z observed within the pair of doublet SO states of $[Dy(Por)(L3)]^+$. This change is much smaller, approximately 18 times smaller, than the observed change in $[Dy(Por)(L4)]^+$. This suggests that the change of the second ligand influences $L_Z(\pi)$, consequently leading to a different interaction with **J**. Ground state calculations indicate that the main magnetic axis of *Jz* in $[Dy(Por)(L3)]^+$ is not

perpendicular to the porphyrin part, potentially contributing to this effect.

Furthermore, the presence of multiple energy levels between doublets 133 and 142 in $[Dy(Por)(L3)]^+$ poses challenges for determining the Δ_{JL} value via half-energy separation, a method previously employed in other studies. Despite this limitation, the current calculation provides a qualitative assessment of the **J-L** interaction, which was previously beyond reach.

In addition, we have successfully identified, for the first time, the SO states associated with $\pi \rightarrow \pi^*$ transitions in the B band. These states are separated by 47288 cm^{-1} and 47299 cm^{-1} for $[Dy(Por)(L4)]^+$ and at 46815 cm^{-1} and 47091 cm^{-1} for $[Dy(Por)(L3)]^+$ from their ground states. Notably, these SO states exhibit significantly high oscillator strength and are confidently assigned to the B band, as shown in Tables 2 and 3. This substantial oscillator strength aligns with the characteristic behavior of the B band in porphyrin/metalloporphyrin compounds. Regarding changes in angular momentum, the disparity in angular momentum between their doublet excited SO states and their lowest doublet SO states are marginal (<0.1). These results correspond with computational findings on $[Y(Por)(L4)]^+$ and $[Y(Por)(L3)]^+$ ($L_Z(\pi)$ Q≈4.0, $L_Z(\pi)$ B≈0.1). Additionally, their doublet excited SO states demonstrate negative changes in angular momentum compared to their lowest doublet SO state, indicating an antiferromagnetic-type **J-L** interaction in the B band. Furthermore, these computational outcomes qualitatively support our experimental findings.

4. Conclusion

The study explores the electronic structures of $[Dy(Por)(L)]^+$ complexes in both ground and excitedstates using the CASSCF method. Results revealed significant changes in sublevel structure upon replacing nitrogen with oxygen in the capping ligand, leading to variations in the energy separation between the lowest and second lowest substates. Particularly, $[Dy(Por)(L3)]^+$ exhibits a deviation in the main magnetic axis orientation compared to other complexes, underlining ligand sensitivity in symmetry. Additionally, the study identifies SO states associated with $\pi \rightarrow \pi^*$ transitions in the Q and B bands. Furthermore, it confirms the presence of an antiferromagnetic-type **J-L** interaction between the orbital angular momentum generated by π and the total angular momentum of the dysprosium ion in $[Dy(Por)(L3)]^+$ and $[Dy(Por)(L4)]^+$ complexes.

Acknowledgements

All calculations have been done using supercomputer system SQUID at the Cybermedia Center, Osaka University.

References

(1) K. Kizaki, et al., *Chem. Commun.,* **53**, 6168-6171, (2017); T. Fukuda, et al., *Chem. Eur. J.*, **23**, 16357-16363, (2017).

(2) A. Santria, サイバーメディア HPC ジャーナル. 2023, 13, p. 45- 49

(3) Avogadro: an open-source molecular builder and visualization tool. Version 1.1.1 ; M.D. Hanwell, et al., *journal of Cheminformatics*, **4**, 1-17 (2012)

(4) M. J. Frisch, et al., Gaussian, Inc., Wallingford CT, 2019.

(5) G. A. Petersson, et al., *J. Chem. Phys.,* **94**, 6081-6090, (1991).

(6) M. Dolg, et al., *J. Chem. Phys.,* **90**, 1730-1734, (1989).

(7) I. F. Galvan, et al., *J. Chem. Theory Comput.,* **15**, 5925-5964, (2019).

(8) A. Santria, et al., *Dalton Trans.*, **48**, 7685-7692 (2019).

(9) A. Santria, et al., *Inorg. Chem.,* **59**, 14326-14336 (2020).

(10) L.C. Adi, et al., *Dalton Trans.*, **53**, 628-639 (2024)